Thin-Walled Structures 185 (2023) 110567

Contents lists available at ScienceDirect

Thin-Walled Structures

journal homepage: www.elsevier.com/locate/tws

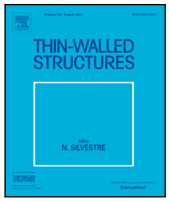

# Tests of concrete-filled high strength steel RHS and SHS beams

Yun-Qiao Deng [a,1], Yuner Huang [b,*], Ben Young [c]

[a] Department of Civil Engineering, The University of Hong Kong, Pokfulam Road, Hong Kong, China
[b] School of Engineering, University of Edinburgh, Edinburgh, Scotland, UK
[c] Department of Civil and Environmental Engineering, The Hong Kong Polytechnic University, Hong Kong, China

ARTICLE INFO

*Keywords:*
Beam
Concrete
Four-point bending tests
High strength steel
Structural design
Tubular

ABSTRACT

This paper presents an experimental investigation of concrete-filled high strength steel tubular (CFHSST) beams. A total of 35 four-point bending tests were conducted, covering high-strength steel square and rectangular hollow sections with nominal 0.2% proof stresses of 700 MPa and 900 MPa. Each high strength steel tubular section was filled with concrete materials of strengths equal to 40, 70 and 110 MPa, respectively. Hollow steel tubes were also tested for comparison purpose. Moment capacity of the test specimens was measured, and ductility of the test specimens was calculated, in order to evaluate the structural benefit associated with the composite action between the two materials. It was shown that both moment capacities and ductility of the CFHSST beams were significantly increased compared to the corresponding hollow sections without concrete infill. It should be noted that the very high strength steel material of 900 MPa is not covered in any design provisions. The current design equations were derived based on normal steel and concrete grades. The suitability of the current design rules, including American Specification (AISC) and European Code (EC4), was assessed for concrete-filled high strength steel tubular sections subjected to bending.

## 1. Introduction

Concrete and steel are the two most commonly used construction materials, but the production of cement and steel releases approximately 6.5% and 7.0% global carbon dioxide ($CO_2$) emissions, respectively [1]. To achieve the goal of net-zero $CO_2$ emissions globally by 2050, it is necessary to investigate efficient use of the two materials in structural members. Concrete-filled steel tubular (CFST) structures have gained increasing interests in research and construction industry, as the two materials complement each other to provide enhancement in structural behaviour [2]. Firstly, the outer steel tube provides confinement for concrete core, which increases its strength and ductility under a triaxial compressive condition [3]. Secondly, concrete core prevents steel tube from inward local buckling under compressive stress [4]. Thirdly, the steel tube can serve as a formwork for concrete casting, which could reduce labour cost and construction time. The structural benefit of CFST in resisting compression is obvious, and they have already been widely used as columns or beam–column members in construction. Previous researches on CFST mainly focused on its structural behaviour under compression with normal strength steel material (nominal yield strength $f_y < 460$ MPa) [5–8]. It was demonstrated that CFST exhibited desirable load-carrying capacity and ductility by utilizing the composite effect in both materials. The effectiveness of steel confinement depends on loading conditions and section slenderness of steel tube. The greatest confinement effect was found when the loading was acting on concrete only with steel tube was used as pure circumferential restrain [4]. Such confinement effect can prevent brittle failure of concrete core and significantly improve ductility in CFST compared to hollow steel tube or reinforced concrete members [9,10]. The ductility of CFST decreased with section slenderness of steel tube [11]. Steel confinement for CFST was found to be effective even for thin-walled steel tubes with reinforcement ratio as low as 4%–6% [12]. On the other hand, the concrete core effectively prevents or delays local buckling of steel tube [4]. A new form of CFST columns confined with internal high strength steel spiral was shown to provide better structural performance than those without confinement [13–15].

Compared with CFST columns, research on CFST members under bending is limited. This is because the structural advantage on CFST flexural members due to composite effect between the two materials is less than those members under axial compression. Concrete is weak in tensile stress, and the confinement by outer steel tube is less effective for members under bending. However, some structural systems such as railway bridge had used CFST members as main girder to provide noise and vibration reduction [16]. Furthermore, members subjected to pure bending is the extreme condition of beam–columns with large eccentricity. Therefore, structural behaviour of CFST beams with normal strength steel was studied [2,17–19]. It was shown that

* Corresponding author.
*E-mail address:* yuner.huang@ed.ac.uk (Y. Huang).
[1] Present address: Atkins China Ltd, Tsim Sha Tsui, Kowloon, Hong Kong, China.

https://doi.org/10.1016/j.tws.2023.110567
Received 9 November 2022; Received in revised form 12 January 2023; Accepted 18 January 2023
Available online 1 February 2023

**Table 1**
Steel and concrete materials in each section.

| Section ($D \times B \times t$) | Steel section class[a] | Steel strength (MPa) | Concrete strength (MPa)[b] |
|---|---|---|---|
| 80 × 80 × 4 | 2, 3 | 700, 900 | 0, 40, 70, 110 |
| 100 × 100 × 4 | 4 | 700, 900 | 0, 40, 70, 110 |
| 100 × 50 × 4 | 1 | 700 | 0, 40, 70, 110 |
| 50 × 100 × 4 | 4 | 700 | 0, 40, 70, 110 |
| 140 × 140 × 5 | 4 | 700 | 0, 40, 70, 110 |
| 120 × 120 × 4 | 4 | 900 | 0, 40, 70, 110 |

[a]Classification based on Table 5.1 of EC3 Part 1-1 (BSI 2005) for hollow steel sections.
[b]Concrete strength = 0 MPa refers to hollow steel tube without concrete infill.

**Table 2**
Measured dimensions of hollow and concrete-filled high strength steel specimens.

| Specimen | $D$ (mm) | $B$ (mm) | $t$ (mm) | $r_i$ (mm) | $L$ (mm) | $A_s$ (mm$^2$) | $A_c$ (mm$^2$) | $D/t$ | $\frac{A_s}{A}$ |
|---|---|---|---|---|---|---|---|---|---|
| H80 × 80 × 4-0 | 80.25 | 80.24 | 3.942 | 5.5 | 1489.8 | 1147 | – | 20.4 | – |
| H80 × 80 × 4-40 | 80.23 | 80.35 | 3.928 | 5.5 | 1491.5 | 1152 | 5221 | 20.4 | 0.18 |
| H80 × 80 × 4-70 | 80.30 | 80.23 | 3.964 | 5.5 | 1490.0 | 1166 | 5207 | 20.3 | 0.18 |
| H80 × 80 × 4-110 | 80.20 | 80.22 | 3.964 | 5.5 | 1491.8 | 1165 | 5199 | 20.2 | 0.18 |
| H100 × 100 × 4-0 | 100.37 | 100.54 | 3.977 | 5.5 | 1489.5 | 1486 | – | 25.2 | – |
| H100 × 100 × 4-40 | 100.37 | 100.46 | 3.951 | 4.6 | 1491.5 | 1457 | 8540 | 25.4 | 0.15 |
| H100 × 100 × 4-70 | 100.54 | 100.51 | 3.968 | 5.3 | 1489.5 | 1482 | 8549 | 25.3 | 0.15 |
| H100 × 100 × 4-110 | 100.30 | 100.49 | 3.965 | 3.5 | 1491.8 | 1498 | 8539 | 25.3 | 0.15 |
| H100 × 50 × 4-0 | 100.38 | 50.09 | 3.984 | 5.3 | 1489.8 | 1093 | – | 25.2 | – |
| H100 × 50 × 4-0R | 100.35 | 50.47 | 3.951 | 6.0 | 1490.3 | 1086 | 3904 | 25.4 | 0.22 |
| H100 × 50 × 4-40 | 100.48 | 50.23 | 3.932 | 5.8 | 1491.0 | 1066 | 3895 | 25.6 | 0.21 |
| H100 × 50 × 4-70 | 100.51 | 50.31 | 3.975 | 5.5 | 1490.0 | 1088 | 3895 | 25.3 | 0.22 |
| H100 × 50 × 4-110 | 100.44 | 50.15 | 3.975 | 5.5 | 1490.0 | 1093 | 3877 | 25.3 | 0.22 |
| H50 × 100 × 4-0 | 50.30 | 100.46 | 3.960 | 5.8 | 1490.5 | 1091 | – | 12.7 | – |
| H50 × 100 × 4-40 | 50.19 | 100.40 | 3.923 | 6.0 | 1490.5 | 1077 | 3888 | 12.8 | 0.22 |
| H50 × 100 × 4-40R | 50.11 | 100.36 | 3.964 | 4.8 | 1491.0 | 1080 | 3879 | 12.6 | 0.22 |
| H50 × 100 × 4-70 | 50.12 | 100.39 | 3.971 | 6.0 | 1490.5 | 1077 | 3868 | 12.6 | 0.22 |
| H50 × 100 × 4-110 | 50.27 | 100.45 | 3.958 | 5.5 | 1490.8 | 1079 | 3893 | 12.7 | 0.22 |
| H140 × 140 × 5–0 | 139.94 | 140.61 | 4.902 | 7.8 | 1790.0 | 2583 | – | 28.5 | – |
| H140 × 140 × 5–40 | 139.90 | 140.64 | 4.926 | 8.0 | 1790.3 | 2622 | 16 954 | 28.4 | 0.13 |
| H140 × 140 × 5–70 | 139.81 | 140.59 | 4.932 | 9.0 | 1791.0 | 2619 | 16 918 | 28.3 | 0.13 |
| H140 × 140 × 5–110 | 139.94 | 140.76 | 4.927 | 8.3 | 1790.0 | 2604 | 16 970 | 28.4 | 0.13 |
| V80 × 80 × 4-0 | 80.11 | 80.38 | 3.952 | 7.0 | 1489.8 | 1157 | – | 20.3 | – |
| V80 × 80 × 4-40 | 80.17 | 80.40 | 3.954 | 6.0 | 1491.8 | 1156 | 5208 | 20.3 | 0.18 |
| V80 × 80 × 4-70 | 80.16 | 80.39 | 3.957 | 6.0 | 1490.0 | 1153 | 5205 | 20.3 | 0.18 |
| V80 × 80 × 4-110 | 80.04 | 80.25 | 3.921 | 7.0 | 1490.0 | 1134 | 5186 | 20.4 | 0.18 |
| V100 × 100 × 4-0 | 100.56 | 100.02 | 3.971 | 8.3 | 1487.8 | 1485 | – | 25.3 | – |
| V100 × 100 × 4-40 | 100.62 | 100.00 | 3.940 | 8.0 | 1491.3 | 1522 | 8466 | 25.5 | 0.15 |
| V100 × 100 × 4-70 | 100.19 | 99.83 | 3.964 | 7.5 | 1489.8 | 1497 | 8402 | 25.3 | 0.15 |
| V100 × 100 × 4-70R | 100.54 | 100.05 | 3.961 | 8.0 | 1490.0 | 1521 | 8455 | 25.4 | 0.15 |
| V100 × 100 × 4-110 | 100.39 | 100.02 | 3.957 | 7.8 | 1491.3 | 1515 | 8448 | 25.4 | 0.15 |
| V120 × 120 × 4-0 | 120.99 | 120.83 | 3.910 | 8.0 | 1689.0 | 1827 | – | 30.9 | – |
| V120 × 120 × 4-40 | 121.08 | 120.88 | 3.928 | 6.5 | 1686.7 | 1846 | 12738 | 30.8 | 0.13 |
| V120 × 120 × 4-70 | 121.06 | 120.86 | 3.913 | 5.3 | 1684.5 | 1832 | 12754 | 30.9 | 0.13 |
| V120 × 120 × 4-110 | 121.08 | 120.84 | 3.938 | 7.3 | 1687.8 | 1851 | 12714 | 30.7 | 0.13 |

**Table 3**
Chemical composition in high strength steel.

| Steel grade | CEV (%) | C (%) | Si (%) | Mn (%) | P (%) | S (%) | Al (%) | Nb (%) | V (%) | Cu (%) | Cr (%) | N (%) | Ti (%) | Mo (%) | Ni (%) | B (%) |
|---|---|---|---|---|---|---|---|---|---|---|---|---|---|---|---|---|
| OPTIM 700 PLUS MH | 0.37 | 0.06 | 0.20 | 1.78 | 0.007 | 0.003 | 0.034 | 0.082 | 0.015 | 0.025 | 0.052 | 0.004 | 0.110 | 0.007 | 0.040 | 0.0003 |
| OPTIM 900 QH | 0.47 | 0.08 | 0.20 | 1.05 | 0.010 | 0.002 | 0.037 | 0.002 | 0.012 | 0.017 | 0.899 | 0.005 | 0.030 | 0.142 | 0.078 | 0.0023 |

CFST members under bending behaved more ductile, as the concrete core changed failure mode of the outer steel tube allowing further deformation and load carrying after occurrence of local buckling, while the steel tube confinement reduced formation of cracks in concrete core [2]. However, enhancement in bending strength due to composite action is less than CFST compression members [11]. Design rules in EC4 and CIDECT were found to be capable of providing accurate prediction for flexural strengths of CFST circular sections with normal strength steel and concrete materials, and can be conservatively extended to a new range of section slenderness ($100 < \lambda_s < 188$) [17], where $\lambda_s$ is the section slenderness given by $(d/t)(f_y/250)$, and $d$, $t$ and $f_y$ are the diameter, wall thickness, and yield strength of steel tube respectively.

In recent decade, steel manufacturing technology has been improved, which produces high strength steel (HSS) tubes with 0.2% proof stress (yield strength, $f_y$) as high as 1360 MPa feasible and more economical [20]. Furthermore, application of high strength concrete in construction industry becomes more common. Concretes with a characteristic strength of 60–100 MPa or even 120 MPa were commercially developed in 1990s and have nowadays been used in the construction of high-rise buildings and bridges in many parts of the

**Table 4**
Ingredient and properties of concrete-filled in high strength steel tubes.

| | Concrete grade | | | | | |
|---|---|---|---|---|---|---|
| | C40 | | C70 | | C110 | |
| | Batch I | Batch II | Batch I | Batch II | Batch I | Batch II |
| Fine aggregate (kg/m$^3$) | 1286 | 1286 | 1143 | 1143 | 942 | 942 |
| Cement (kg/m$^3$) | 600 | 600 | 846 | 846 | 878 | 878 |
| Water (kg/m$^3$) | 312 | 312 | 288 | 288 | 224 | 224 |
| Superplasticizer (kg/m$^3$) | 1.21 | 1.16 | 3.88 | 3.84 | 37.47 | 39.03 |
| Silica fume (kg/m$^3$) | – | – | – | – | 220 | 220 |
| Water/cement ratio | 0.52 | 0.52 | 0.34 | 0.34 | 0.20 | 0.20 |
| Paste volume | 50% | 50% | 56% | 56% | 63% | 63% |
| Slump (mm) | 260 | – | 235 | – | 260 | – |
| Span (mm) | 506 | – | 503 | – | 533 | – |
| Cylinder strength (MPa) | 46.0 | 46.6 | 71.6 | 70.7 | 117.3 | 116.6 |
| Number of tests | 5 | | 5 | | 5 | |
| Coefficient of variation | 0.066 | | 0.038 | | 0.056 | |
| Mean of measured strength (MPa) | 46.3 | | 71.2 | | 117.0 | |

world [21]. There has been an increasing research interests in exploring the potential of using high strength steel materials in CFST members [22–29]. However, the application of concrete-filled cold-formed high strength steel in construction industry is still limited because there is no adequate design guidance. Design standards for CFST column members, such as EC4 [30], American Specification AISC 360-16 [31] and Chinese code DBJ/T [32], were developed for normal strength concrete and steel materials, and thus they may not be applicable for high strength materials. In general, concrete-filled high strength steel tubular (CFHSST) members share some common structural behaviour with their counterparts of normal strength steel, such as enhancement of flexural capacity and ductility [33,34]. However, it should be noted that the use of high strength concrete reduced member ductility, compared with normal strength concrete. However, the ductility behaviour could be improved by confining the concrete core with high strength steel tube [11]. Furthermore, CFST columns filled with ultra-high strength concrete with low steel ratio may be very brittle and the confinement effect should be ignored [35]. In other words, CFST with higher strength concrete requires higher strength or thicker steel tube to provide sufficient confinement. The bearing capacity and energy dissipation capacity increased substantially with steel ratio in composite members with high strength steel and high strength concrete under bending [36]. Test results of concrete-filled high strength steel tubes (CFHSST) showed that EC4 approach was unsafe for members under compression [37], while the Chinese Standard DB/T 29-57-2016 [38] was conservative for rectangular shape CFHSST columns [23]. Experimental and analytical investigation was performed on square concrete-filled high strength steel tubular (CFHSST) members consisting of high strength steel ($f_y$ = 325 – 900 MPa) and high strength concrete ($f_{ck}$ = 80 MPa and 120 MPa) under bending [39]. Results showed that specimens were failed by local buckling on flange or fracture and current design specifications are conservative in predicting ultimate capacity of high strength material. Three CHFSST beam tests were conducted with normal strength concrete ($f_{ck}$ = 30 MPa) and high strength steel ($f_y$ = 750 MPa) [37]. It was shown that the Eurocode 4 [30] overestimated the moment capacity by up to 13%. On the other hand, EC4 [30] and American Specification [30] underestimated moment capacity by 11% and 18% for CFST flexural members with normal strength steel and high strength concrete [18]. Six CFHSST members consisted of high strength concrete and high strength steel were tested under bending [40]. It was shown that the specimens exhibited excellent ductility, and ultimate bearing capacity significantly increases with steel ratio, but less influenced by concrete strength. Experimental and numerical investigation on high strength concrete-filled high strength steel tubular (HSCFHSST) stub columns under combined compression and bending were performed [41]. It was indicated that the existing design rules, including American Specification, Australian/New Zealand Standard and European Code, generally provide accurate or slightly unconservative predictions for the failure loads of HSCFHSST stub columns under combined loading. Design for HSCFHSST and CFHSST columns after exposed to fire were investigated by Zhong et al. [42] and Zhong and Zhao [43], respectively. The results have shown that the existing ambient temperature design rules with post-fire material properties are able to accurately predict post-fire resistance of the column members.

Up to now, research on CFHSST members under bending is still limited. Most of the bending tests reported in literature were part of research on beam–columns, and thus influence of material and geometric parameters on moment capacity and ductility of members under bending were not fully evaluated, especially for CFST members with high strength steel and high strength concrete. However, such components can also take lateral loading or bending in different engineering application. This study aims at providing experimental evidence on flexural behaviour of CFST members fabricated from cold-form high strength steel with nominal yield strengths of 700 and 900 MPa and concrete core with strength ranged from 40–110 MPa. Hollow and concrete-filled steel square and rectangular hollow section members were tested under four-point bending. The main parameters to be evaluated include concrete grade, steel grade, and depth-to-thickness ($D/t$) ratio of the steel tube, where $D$ is the overall depth of the hollow steel sections and $t$ is the thickness. The failure mode, moment capacity, moment–curvature relationship and composite effect were obtained from the test programme and discussed in this paper. Furthermore, suitability of current design equations were also assessed.

## 2. Test specimens

A total of 35 test specimens that consists of cold-formed high strength steel tubes of square and rectangular hollow sections (SHS and RHS) and normal-to-high strength concrete infills were tested under pure bending. The steel tubes include four square hollow sections with dimension ($D \times B \times t$) 80 × 80 × 4,100 × 100 × 4,140 × 140 × 5 and 120 × 120 × 4, where $D$, $B$ and $t$ are depth, width and wall thickness in millimetres, respectively. There was also a rectangular hollow section subjected to major and minor axis bending, which was represented by 100 × 50 × 4 and 50 × 100 × 4, respectively. The steel sections covered all four classes determined based on EC3 Part 1-1 [44], as shown in Table 1. The section 80 × 80 × 4 was classified as Class 2 and 3 when the yield strength equalled to 700 MPa and 900 MPa, respectively.

The test specimens were labelled such that the material used for the tubes, steel tube cross-sectional dimensions and the infilled concrete grades, as shown in Table 2. An example is the specimen ID "V80 × 80 × 4-40", where "V" stands for V-series of very HSS with nominal yield strength 900 MPa, followed by the nominal cross-section dimension of the tube that had a depth of 80 mm, width of 80 mm and thickness of 4 mm, and "-40" refers to grade of the infilled concrete C40. The hollow steel beams without concrete infill were marked with "-0". In addition, the letter "R" in the label indicates repeated test of the

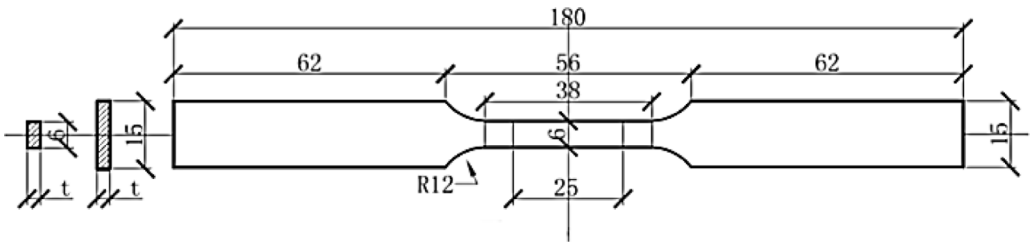


**Fig. 1.** High strength steel coupon dimensions.

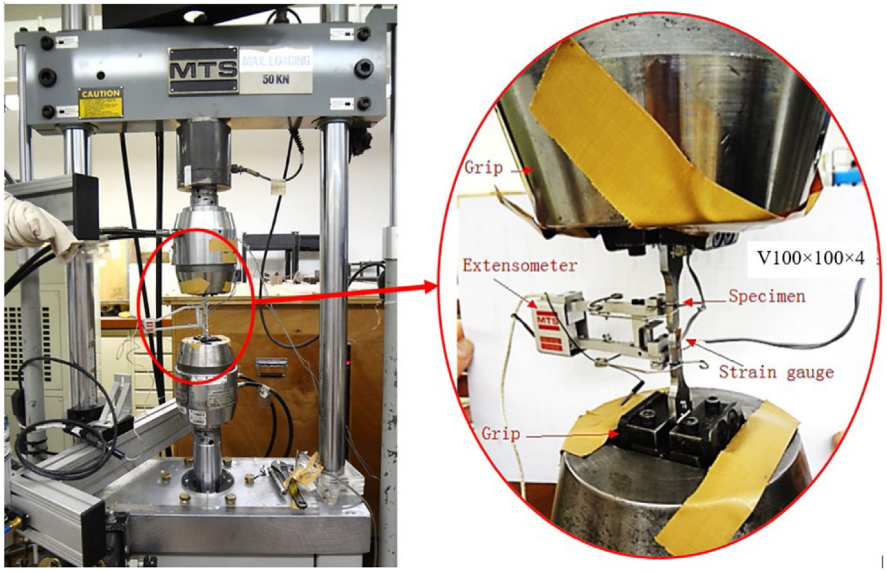


**Fig. 2.** Test set-up of coupon test.

identical specimen. Repeat tests were conducted to check the reliability of the test results.

The measured dimensions of the HSS sections are shown in Table 2, where $r_i$ is the inner corner radius and $L$ is the specimen length. The measured values of overall depth-to-thickness ($D/t$) ratio of these tubes ranged from 12.6 to 30.9. The steel ratio ($A_s/A$), defined by steel area ($A_s$) over the total cross-sectional area ($A$) of the composite section, ranged from 0.13 to 0.22. The specimen lengths ranged from 1487.8 to 1791.0 mm.

The steel tubes were cold-formed from high strength steel (HSS) material with nominal yield strength equalled to 700 MPa (Grade OPTIM 700 PLUS MH) or 900 MPa (Grade OPTIM 900 QH), labelled as H-series and V-series respectively in this study. The HSS material adopted in this study was complied with the BS EN 10 204 [45]. The chemical compositions of these HSS obtained from milling certificates are shown in Table 3.

Normal strength and high strength concrete were used in this study to fill the steel tubes. Three grades of concrete were used with the compressive strengths of 40, 70 and 110 MPa, as shown in Table 1. For the high strength concrete, condensed silica fume was used to replace a certain portion of ordinary Portland cement. The ordinary Portland cement of strength class 52.5 N and complying with BS 12 [46] was used. Due to the volume constraints of the concrete mixer and in order to achieve the best mixing quality, each grade of concrete was divided into two batches (Batch I and Batch II) to fill the SHS and RHS tubes, respectively. The concrete mixture ingredients are shown in Table 4. In order to make sure the concrete filled the tubular specimens completely, especially the smallest sections, crushed granite rock with a nominal maximum size of 5 mm was used as fine aggregate. Considering the relatively small section size of the steel tubes, concrete material was designed to have a high flowability with a high paste

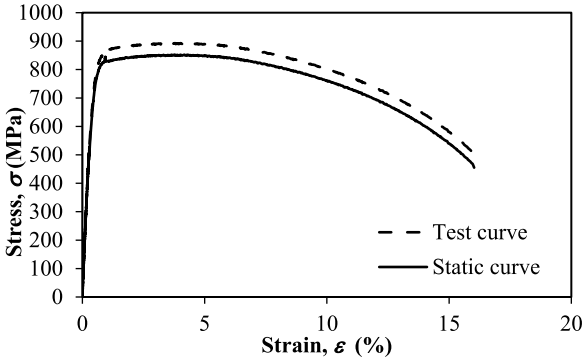


**Fig. 3.** Test and static stress–strain curves for coupon specimen H80 × 80 × 4.

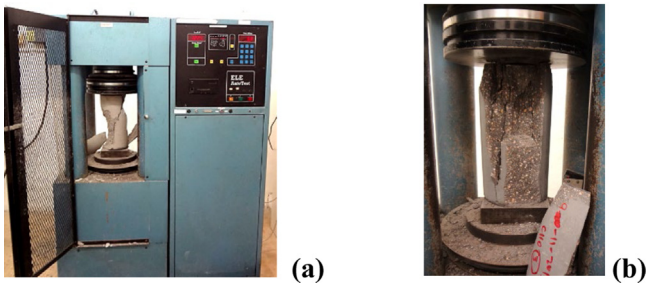


**Fig. 4.** (a) Concrete compressive test; (b) brittle failure of C110 concrete.

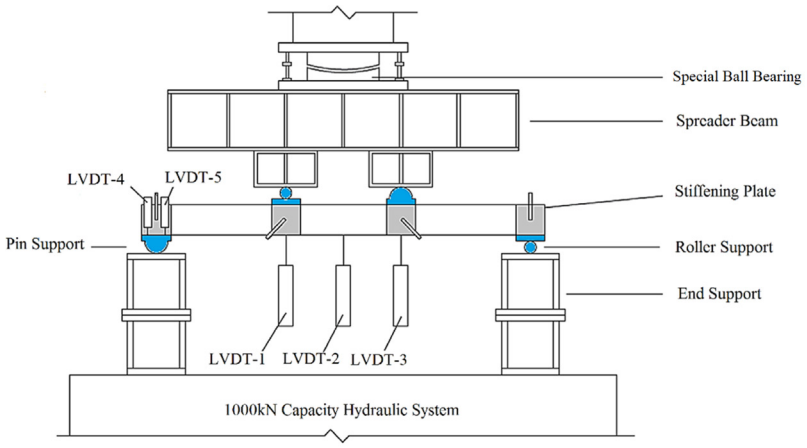


(a)

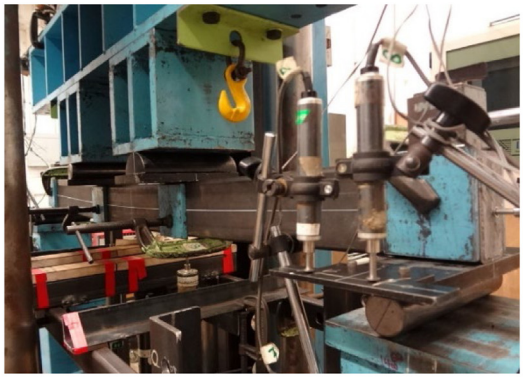

(b)

**Fig. 5.** Four-point bending test setup (a) Schematic view (b) Actual beam test.

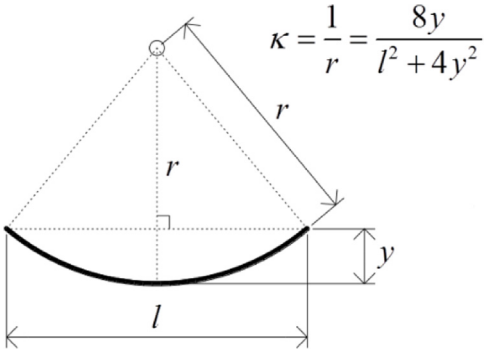


**Fig. 6.** Calculation of curvature using LVDTs.

volume ratio of 50%–63%. A third generation polycarboxylate-based superplasticizer was added to enhance the flowability and workability of the fresh concrete.

## 3. Material tests

### 3.1. Cold-formed high strength steel

Tensile coupon tests were conducted to obtain material properties of the cold-formed high strength steel tubes. The tests were conducted according to Australian Standard AS 1391 [47], American Standard ASTM [48] and recommendations by [49]. Flat tensile coupons were extracted from SHS and RHS at the web 90° angle from the seam weld and away from the corner region, in order to avoid the influence of welding or cold-working effects on the test results. Coupon dimensions conform to the ISO 6892-1 [50], AS 1391 [47] and ASTM [48] with a gauge length of 25 mm, as shown in Fig. 1.

The tensile coupons were tested in a 50 kN capacity MTS testing machine. The flat ends of the specimens were gripped by clamping, as shown in the test set-up in Fig. 2. The load was measured by a built-in load cell of the MTS machine, and deformation was measured by an extensometer and two strain gauges attached to both faces at the mid-length of the coupon. Tensile force was applied by displacement control with loading rates of 0.05 mm/min for the initial elastic portion, which was then increased to 0.3 mm/min and 0.5 mm/min after yielding and ultimate strength, respectively, until the coupons fracture. Metallic materials are generally sensitive to loading rates. Mechanical properties of steel material under static load can be obtained by holding the strain during testing [51]. In this study, straining was paused for 90 s when the loading reached yield and ultimate strengths to obtain the corresponding static loads, which were used to derive static stress–strain curve [49], as shown in Fig. 3.

Material properties, such as Young's modulus of steel ($E_s$), static 0.2% proof stress ($\sigma_{0.2}$), static ultimate tensile strength ($\sigma_u$), strain at fracture ($\varepsilon_f$) and Ramberg–Osgood parameter ($n$) were obtained, as summarized in Tables 5 and 6 for H- and V-series high strength steel materials, respectively. The Ramberg–Osgood parameter ($n$) was calculated as $\ln(0.01/0.2)/\ln(\sigma_{0.01}/\sigma_{0.2})$, where $\sigma_{0.01}$ and $\sigma_{0.2}$ are the 0.01% and 0.2% proof stresses. Repeated tests were conducted for specimens H100 × 100 × 4 and H140 × 140 × 5, which were denoted with "R" or "R2" at the end of the specimen label.

The $\sigma_{0.2}$ of flat coupons ranged from 682 MPa to 762 MPa with an average of 721 MPa for grade 700 MPa steel (H-series); and ranged

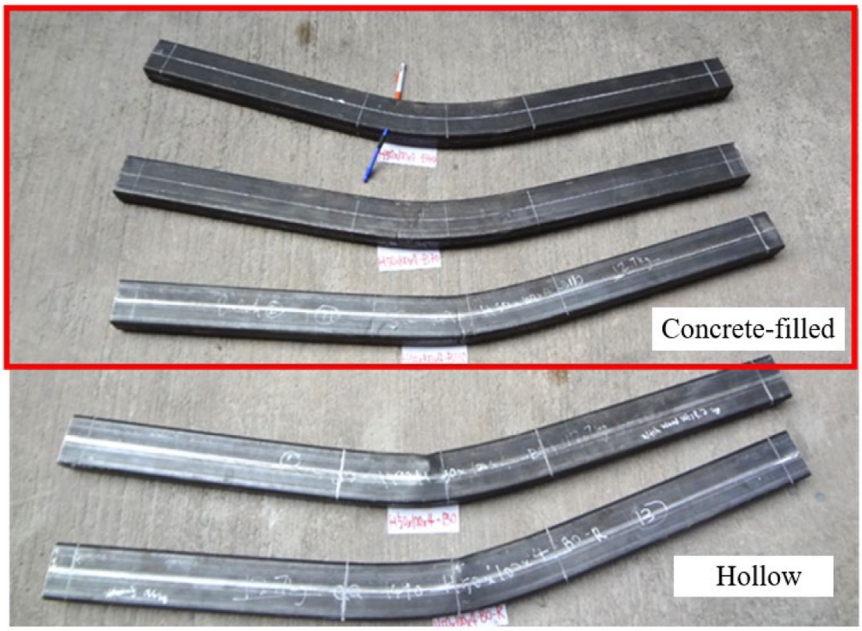


(a)

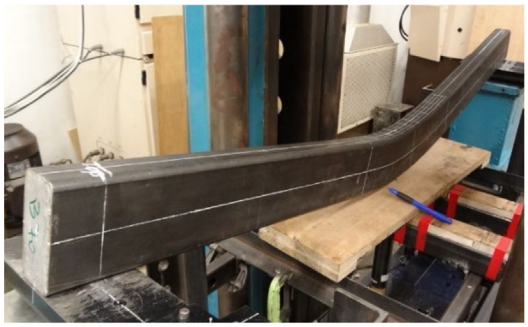

(b)

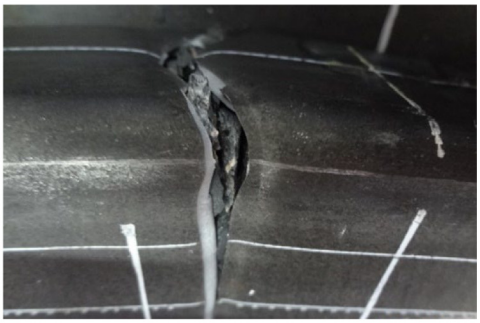

(c)

**Fig. 7.** Failed beam specimens (a) Comparison of failed concrete-filled and hollow specimens; (b) Flexural failure; (c) Steel fracture.

**Table 5**
H-series high strength steel material properties obtained from coupon tests.

| Section ($D \times B \times t$) | $\sigma_{nominal}$ (MPa) | $E_s$ (GPa) | $\sigma_{0.2}$ (MPa) | $\sigma_u$ (MPa) | $\varepsilon_f$ (%) | $n$ |
|---|---|---|---|---|---|---|
| H80 × 80 × 4 | 700 | 219 | 756 | 852 | 16.0 | 3.2 |
| H100 × 50 × 4 | 700 | 218 | 721 | 842 | 14.7 | 2.3 |
| H100 × 100 × 4 | 700 | 218 | 722 | 819 | 18.0 | 3.3 |
| H100 × 100 × 4-R | 700 | 216 | 762 | 819 | – | 3.4 |
| H140 × 140 × 5 | 700 | 209 | 682 | 822 | 22.0 | 3.0 |
| H140 × 140 × 5-R | 700 | 215 | 715 | 820 | 21.0 | 4.1 |
| H140 × 140 × 5-R2 | 700 | 207 | 692 | 842 | 21.3 | 2.7 |

**Table 6**
V-series high strength steel material properties obtained from coupon tests.

| Section ($D \times B \times t$) | $\sigma_{nominal}$ (MPa) | $E_s$ (GPa) | $\sigma_{0.2}$ (MPa) | $\sigma_u$ (MPa) | $\varepsilon_f$ (%) | $n$ |
|---|---|---|---|---|---|---|
| V80 × 80 × 4 | 900 | 211 | 1022 | 1179 | 11.8 | 3.7 |
| V100 × 100 × 4 | 900 | 203 | 980 | 1092 | 12.1 | 4.8 |
| V120 × 120 × 4 | 900 | 204 | 991 | 1140 | 12.2 | 3.9 |

from 980 MPa to 1022 MPa with an average of 998 MPa for grade 900 MPa steel (V-series). The ultimate tensile strengths ranged from 819 MPa to 852 MPa with an average of 831 MPa for grade 700 MPa steel (H-series), and ranged from 1092 MPa to 1179 MPa with an average of 1137 MPa for grade 900 MPa steel (V-series). The elongations at fracture were ranged from 14.7% to 22% and 11.8% to 12.2% for the H-series and V-series, respectively.

Mechanical properties at corner regions of cold-formed SHS and RHS are higher than those obtained from the flat regions, due to strength enhancement during cold-forming process. Ma et al. [52]

conducted tensile coupon tests at the corner regions of the same batch of steel tubes as those in this study. It is shown that the Young's modulus of corner and flat coupons in the same series is similar. The 0.2% proof stress of the corner coupons are 18%–29% and 14%–18% higher than the flat coupons of H- and V-series, respectively.

### 3.2. Concrete

Slump tests were conducted to ensure workability of fresh concrete before filling the steel tubes. Sufficient workability of the test specimens was indicated by the results of the large slump at about 250 mm, and the span at about 500 mm, as shown in Table 4. Trial tests were conducted to examine the quality of concrete infill in the smallest section. The trial steel tubes with concrete infill were cut out to ensure the quality of concrete infill.

The unconfined concrete strengths were determined by compressing the plain concrete cylinders (150 mm diameter × 300 mm height), as shown in Fig. 4(a). A brittle failure mode owing to splitting of the concrete was observed for high strength concrete grade C110 with the compressive strength of 110 MPa (Fig. 4(b)). The concrete cylinders were tested at 28 days after casting which is also the first day of the composite beam tests, in the middle of the test program, and also on the day of the last composite beam test for each grade of concrete. The average measured concrete cylinder strengths were 46.2 MPa, 71.2 MPa and 117.0 MPa for the concrete grades of C40, C70 and C110, respectively, as reported in Table 4. Fresh concrete was used to fill the HSS tubes right after concrete mixing.

## 4. Four-point bending tests

A total of 35 tests were conducted on hollow or concrete-filled high strength specimens, among which 22 of these test specimens belonged to H-series high strength steel of SHS and RHS, and 13 specimens belonged to V-series very high strength steel of SHS, as shown in Table 2.

### 4.1. Test method

The tests were conducted in an MTS hydraulic testing system with capacity of 1000 kN. The schematic view of beam test arrangements and the actual beam test are shown in Fig. 5. The beam specimens were simply supported at both ends. Round bars and half-rounded supports were used at the loading points and supports to simulate the roller and pinned conditions. Two point-loads were applied on the specimen through a spreader beam. A special ball bearing sat between the spreader beam and the hydraulic machine, which was used to ensure that there was no gap in the test setup, such that the loading was applied vertically to the beam test specimens. A displacement control loading mode with a loading rate of 2.5 mm/min was applied.

External stiffening plates were clamped to the two sides of the SHS and RHS specimens at the loading points and end support points to prevent localized failure due to high bending moment and/or shear force. The moment span ($L_m$) was fixed at 400 mm and the shear spans ($L_s$) were long enough so that the ultimate cross-sectional bending moment capacity was expected to be reached first before shear failure.

The vertical displacement, end rotation and concrete slip between the steel tube and infilled concrete at the ends of specimen were measured by linear variable displacement transducers (LVDT). Three LVDTs with 100 mm stroke were put on the tension side of specimen within the moment span to measure vertical displacement at mid-span and loading points. The average curvature can be calculated from the readings of these three LVDTs. The curvature $\kappa$ along the moment span was assumed to be constant when the moment span was under a constant bending moment. The averaged curvature of moment span

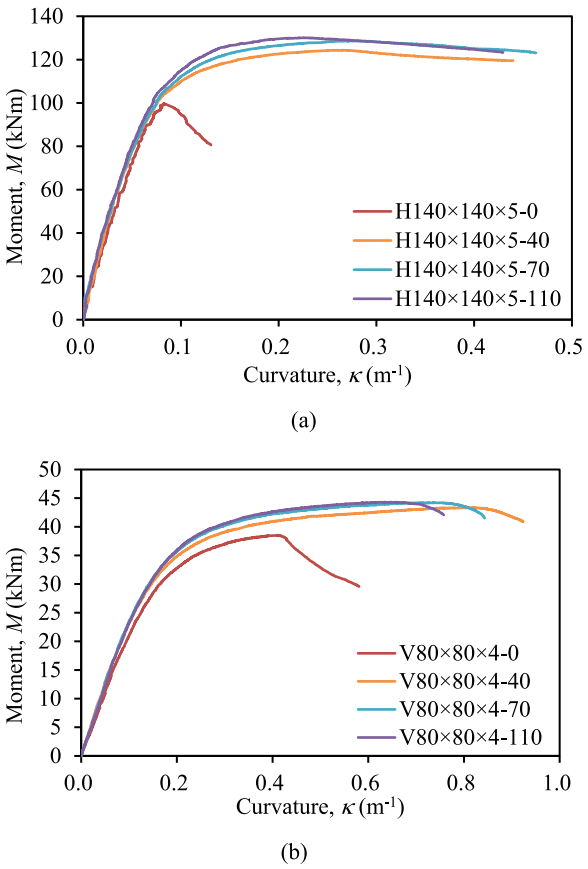


**Fig. 8.** Beam test curves for (a) series H140 × 140 × 5; (b) series V80 × 80 × 4.

can be calculated from the deflection of moment span using Eq. (1) derived from Fig. 6.

$$\kappa = \frac{1}{r} = \frac{8y}{l^2 + 4y^2} \tag{1}$$

where $r$ is the radius of curvature, $l$ is length of moment span and $y$ is the deflection in the moment span. Additional four LVDTs were set on two end support bearing plates to capture the end rotations, as shown in Fig. 5.

### 4.2. Test results

Typical failure modes for hollow and concrete-filled specimens are shown in Fig. 7. It is shown that the concrete-filled specimens could sustain a much larger deformation compared to the hollow specimens. Some composite beams made of very high strength steel and high strength concrete failed by fracture of the steel tubes, where the loading suddenly dropped and the test stopped immediately, as shown in Fig. 7(b).

The experimental moment capacity ($M_{exp}$) was calculated using the ultimate load and the moment span. The experimental moment capacities ($M_{exp}$) of the hollow and CFHSST beam test specimens are summarized in Table 7. The moment–curvature curves of the beam series H140 × 140 × 5 and V80 × 80 × 4 with different concrete grades were plotted in Fig. 8. The moment capacities of the concrete-filled specimens were compared with the moment capacity of the corresponding hollow specimens ($M_{hollow}$), as shown in Table 7. The moment capacity of the concrete-filled beams in this study was found to be 9%–45% larger than the moment capacity of the hollow beams for SHS and RHS. Generally, the moment capacity slightly increased as the concrete strength increased. It has been observed that the effect of different

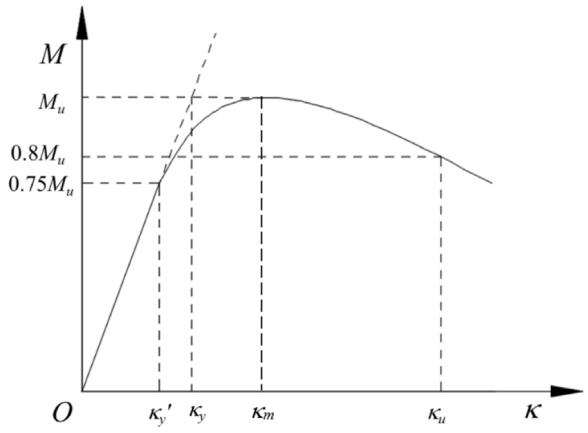


**Fig. 9.** Moment versus curvature diagram.

concrete strengths on the moment capacity was not significant. The effects of differences in concrete strengths were more obvious on the specimens with larger $D/t$ ratio or smaller steel ratio. The test results showed that the concrete core effectively increases moment capacity. On the other hand, the steel tube is also taking up tensile load.

The flexural stiffness is the resistance of a member against bending deformation, and it is a function of elastic modulus and second moment of area of the cross-section. The flexural stiffness ($EI_{exp}$) was determined from the initial slope of the moment–curvature curve for each specimen, as summarized in Table 8. The CFHSST specimens behaved in a very ductile manner. The curvature ductility factor $\mu_c$, reported by Lam et al. [53], was used to quantify the flexural ductility of the beam specimens. Curvature ductility factor $\mu_c$ was calculated by Eq. (2), as summarized in Table 8.

$$\mu_c = \frac{\kappa_u}{\kappa_y} \tag{2}$$

where $\kappa_u$ is the ultimate curvature when the resisting moment dropped to a value of $0.8M_u$ after reaching the ultimate moment $M_u$. In some cases, the beams exhibited excessive deformations while sustained at the ultimate load until fracture of the steel tubes or the tests terminated. For these cases, the maximum recorded curvatures were taken as $\kappa_u$. The value $\kappa_y$ was the yield curvature that was proportional to the value of $M_u$ with the secant stiffness at the resisting moment of $0.75M_u$. It was calculated by $\kappa_y = \kappa_y'/0.75$, where $\kappa_y'$ is the curvature at $0.75M_u$, as explained in Fig. 9. The value $\kappa_m$ was the curvature corresponding to ultimate moment $M_u$. The values of $\kappa_y$, $\kappa_m$ and $\kappa_u$ of each test specimen were summarized in Table 8. It is shown clearly that the concrete-filled specimens had larger curvature than the hollow specimens. Therefore, the CFHSST members were found to be more ductile than the hollow specimens. Generally speaking, the CFHSST specimens had an enhanced flexural strength, larger flexural stiffness and favourable ductility over the hollow high strength steel specimens.

## 5. Design prediction and comparison with test results

### 5.1. Theoretical elastic and plastic moment capacities

The theoretical moment capacity of a beam can be calculated from the distribution of normal stress. It has been established that the cross-section of a beam in pure bending remains in plane and the normal stress varies in proportion to the distance from the neutral axis in the linear elasticity stage. The bending moment in the beam when the maximum stress just reaches the yield stress is the elastic moment $M_{el}$. It was calculated as the maximum stress at the tensile extreme fibre of steel tube reached the yield strength $f_y$. When the stress increases further beyond the yielding stress, the bending moment will continue to increase beyond the elastic moment. When the beam reaches the idealized fully plastic stage where the whole cross-section sustaining the yield stress, this moment is called the plastic moment $M_{pl}$. In this study, the $M_{pl}$ of the concrete-filled tubular (CFT) beam was calculated from the full yield stress distribution across the steel cross-section and the full compressive stress distribution across the concrete cross-section. The tensile stress of concrete portion below the neutral axis was omitted in the calculation of both $M_{el}$ and $M_{pl}$.

The elastic and plastic moment capacities $M_{el}$ and $M_{pl}$ were compared with the 35 test results, as presented in Table 7. It is shown that the elastic moment was very conservative, while the plastic moment provided a closer prediction. The mean value and coefficient of variation (COV) of $M_{exp}/M_{el}$ are 1.40 and 0.101, while those of $M_{exp}/M_{pl}$ are 1.15 and 0.071, respectively. It suggests that materials in the cross-sections of the test specimens generally reach yield strength, which is close to the plastic stress distribution. The moment capacities obtained from the tests were on average 15% higher than plastic moment of the composite section due to composition actions between the two materials as well as the post-yielding strengths and enhanced strength in the corner regions of the steel sections.

### 5.2. Design specification

Design specifications are available for CFT structures, which provide guidelines for predicting moment capacities of concrete-filled composite flexural member. American Specification [31] and European Code 4 [30] are widely used in the construction industry. However, they are based on previous investigations of CFT members made of normal strength steel and normal strength concrete. The applicability of these two codes for CFHSST flexural members beyond the prescribed limits were evaluated by comparing the experimental moment capacities to the design predictions. The measured cross-section dimensions, 0.2% proof stresses of the hollow steel tubes, and the measured cylinder compressive strengths of concrete material were used in the calculation of design strengths.

#### 5.2.1. American specification

The test flexural strengths of concrete-filled specimens were compared with design strengths $M_{AISC}$ calculated based on the design rules in the American Specification ANSI/AISC 360-16 [31] which apply for CFT beams of hot-rolled carbon steel tubes. It should be noted that cold-formed carbon steel tubes were used in this study. The AISC specifies section slenderness by the width-to-thickness ratio ($b/t$, $d/t$ for SHS and RHS), and uses section slenderness limits to classify filled composite members into compact, non-compact or slender sections. Corresponding formulae are provided to determine the nominal moment capacities for CFT members of different section classes. For the CFT of compact sections, the nominal moment $M_n$ was taken as the plastic moment $M_p$, corresponding to the case where the plastic stress distribution over the composite cross-section with maximum concrete compressive stress was limited to $0.85f_c'$, as shown in Fig. 10(a). It should be noted that all the steel tubes in this study are classified as compact sections.

For non-compact sections, $M_n$ is calculated by interpolation between the $M_p$ and yield moment $M_y$, such that

$$M_n = M_p - \left(M_p - M_y\right)\left(\frac{\lambda - \lambda_p}{\lambda_r - \lambda_p}\right) \tag{3}$$

where $M_y$ is the moment corresponding to the yielding of the tension flange and first yield of the compression flange, assuming a linear elastic stress distribution; and $\lambda$, $\lambda_p$ and $\lambda_r$ are slenderness ratios determined from Table I1.1b of the AISC [31]. The maximum concrete compressive stress is limited to $0.7f_c'$ and the maximum steel stress is limited to yield stress $f_y$, as shown in Fig. 10(b). For slender sections, $M_n$ is determined as the first yield moment with compression flange stress limited to the local buckling stress $f_{cr}$ [31], as specified in Eq. (4);

$$f_{cr} = 9E_s/(b/t)^2 \tag{4}$$

**Table 7**
Test results of beam specimens.

| Specimen | $M_{exp}$ (kNm) | $\frac{M_{exp}}{M_{hollow}}$ | $\frac{M_{exp}}{M_{el}}$ | $\frac{M_{exp}}{M_{pl}}$ | $\frac{M_{exp}}{M_{AISC}}$ | $\frac{M_{exp}}{M_{EC4}}$ |
|---|---|---|---|---|---|---|
| H80 × 80 × 4-0 | 29.14 | 1.00 | 1.27 | 1.12 | – | – |
| H80 × 80 × 4-40 | 33.10 | 1.14 | 1.45 | 1.19 | 1.20 | 1.20 |
| H80 × 80 × 4-70 | 33.95 | 1.17 | 1.47 | 1.19 | 1.20 | 1.20 |
| H80 × 80 × 4-110 | 34.08 | 1.17 | 1.47 | 1.16 | 1.17 | 1.17 |
| H100 × 100 × 4-0 | 44.04 | 1.00 | 1.25 | 1.10 | – | – |
| H100 × 100 × 4-40 | 50.92 | 1.16 | 1.45 | 1.18 | 1.19 | 1.19 |
| H100 × 100 × 4-70 | 52.02 | 1.18 | 1.47 | 1.17 | 1.18 | 1.18 |
| H100 × 100 × 4-110 | 53.54 | 1.22 | 1.50 | 1.17 | 1.18 | 1.18 |
| H100 × 50 × 4-0 | 31.96 | 1.00 | 1.49 | 1.22 | – | – |
| H100 × 50 × 4-0R | 31.98 | 1.00 | 1.50 | 1.23 | – | – |
| H100 × 50 × 4-40 | 34.79 | 1.09 | 1.62 | 1.26 | 1.27 | 1.27 |
| H100 × 50 × 4-70 | 35.29 | 1.10 | 1.62 | 1.23 | 1.24 | 1.24 |
| H100 × 50 × 4-110 | 35.99 | 1.13 | 1.63 | 1.21 | 1.22 | 1.22 |
| H50 × 100 × 4-0 | 17.46 | 1.00 | 1.19 | 1.10 | – | – |
| H50 × 100 × 4-40 | 20.42 | 1.17 | 1.42 | 1.25 | 1.25 | 1.25 |
| H50 × 100 × 4-40R | 20.24 | 1.16 | 1.40 | 1.23 | 1.24 | 1.24 |
| H50 × 100 × 4-70 | 20.47 | 1.17 | 1.41 | 1.22 | 1.23 | 1.23 |
| H50 × 100 × 4-110 | 21.07 | 1.21 | 1.46 | 1.23 | 1.24 | 1.24 |
| H140 × 140 × 5–0 | 99.64 | 1.00 | 1.20 | 1.06 | – | – |
| H140 × 140 × 5–40 | 124.34 | 1.25 | 1.49 | 1.21 | 1.22 | 1.22 |
| H140 × 140 × 5–70 | 128.67 | 1.29 | 1.54 | 1.22 | 1.23 | 1.23 |
| H140 × 140 × 5–110 | 130.10 | 1.31 | 1.54 | 1.19 | 1.20 | 1.20 |
| V80 × 80 × 4-0 | 38.56 | 1.00 | 1.24 | 1.09 | – | – |
| V80 × 80 × 4-40 | 43.41 | 1.13 | 1.40 | 1.17 | 1.18 | 1.18 |
| V80 × 80 × 4-70 | 44.26 | 1.15 | 1.42 | 1.17 | 1.18 | 1.18 |
| V80 × 80 × 4-110 | 44.33 | 1.15 | 1.44 | 1.15 | 1.16 | 1.16 |
| V100 × 100 × 4-0 | 52.20 | 1.00 | 1.09 | 0.96 | – | – |
| V100 × 100 × 4-40 | 63.51 | 1.22 | 1.34 | 1.10 | 1.11 | 1.11 |
| V100 × 100 × 4-70 | 64.77 | 1.24 | 1.36 | 1.10 | 1.11 | 1.11 |
| V100 × 100 × 4-70R | 64.94 | 1.24 | 1.36 | 1.10 | 1.11 | 1.11 |
| V100 × 100 × 4-110 | 65.99 | 1.26 | 1.38 | 1.09 | 1.10 | 1.10 |
| V120 × 120 × 4-0 | 69.51 | 1.00 | 0.99 | 0.87 | – | – |
| V120 × 120 × 4-40 | 94.60 | 1.36 | 1.34 | 1.10 | 1.10 | 1.10 |
| V120 × 120 × 4-70 | 98.54 | 1.42 | 1.39 | 1.12 | 1.13 | 1.13 |
| V120 × 120 × 4-110 | 100.76 | 1.45 | 1.41 | 1.10 | 1.11 | 1.11 |
| | | # of specimen | 35 | 35 | 26 | 26 |
| | | Mean | 1.40 | 1.15 | 1.18 | 1.18 |
| | | COV | 0.101 | 0.071 | 0.044 | 0.044 |

Note: All composite specimens in this study are classified as compact sections according to AISC (2016).

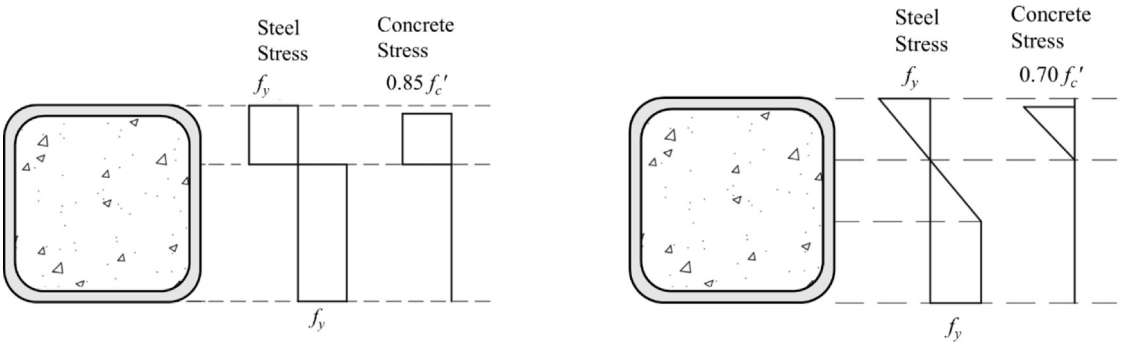


**Fig. 10.** (a) Stress distribution for $M_p$; (b) Stress distribution for $M_y$ [30].

while concrete compressive stress distributes linearly from the neutral axial to extreme compressive fibre of 0.7 $f_c'$.

In this study, the yield stress $f_y$ of the carbon steel was replaced by the 0.2% proof stress of the cold-formed high strength steel material. Nominal moment capacities ($M_{AISC}$) were compared with moment capacities of experimental specimens. The experiment-to-design moment ratios ($M_{exp}/M_{AISC}$) are presented in Table 7. It is shown that the AISC [31] prediction of flexural strengths for CFHSST was quite conservative for the test specimens of compact sections, with the mean value of $M_{exp}/M_{AISC}$ equals to 1.18 and the COV value of 0.044. It is shown that the plastic stress distribution design approach adopted in AISC for compact sections can be further improved by considering the strength enhancement between steel and concrete materials. In addition, the design approaches in AISC for non-compact and slender sections was not evaluated in this study due to the limitation of section dimensions adopted in the test program.

### 5.2.2. European code

The Eurocode 4 [30] determines the design moment resistance $M_{EC4}$ by plastic theory and adopts a full plastic stress distribution in

**Table 8**
Flexural stiffness and ductility of hollow and concrete-filled high strength steel beams.

| Specimen | $EI_{exp}$ (kNm$^2$) | $\kappa_y$ (m$^{-1}$) | $\kappa_m$ (m$^{-1}$) | $\kappa_u$ (m$^{-1}$) | $\mu_c = \frac{\kappa_u}{\kappa_y}$ |
|---|---|---|---|---|---|
| H80 × 80 × 4-0 | 209.73 | 0.16 | 0.41 | 0.67 | 4.19 |
| H80 × 80 × 4-40 | 237.60 | 0.17 | 0.89 | 1.12 | 6.59 |
| H80 × 80 × 4-70 | 248.39 | 0.16 | 0.85 | 1.11 | 6.94 |
| H80 × 80 × 4-110 | 251.25 | 0.17 | 0.66 | 0.92 | 5.41 |
| H100 × 100 × 4-0 | 398.56 | 0.11 | 0.20 | 0.31 | 2.82 |
| H100 × 100 × 4-40 | 463.32 | 0.12 | 0.41 | 0.60 | 5.00 |
| H100 × 100 × 4-70 | 463.05 | 0.12 | 0.40 | 0.52 | 4.33 |
| H100 × 100 × 4-110 | 490.23 | 0.12 | 0.38 | 0.53 | 4.42 |
| H100 × 50 × 4-0 | 240.07 | 0.17 | 0.77 | 1.09 | 6.41 |
| H100 × 50 × 4-0R | 243.78 | 0.16 | 0.79 | 1.12 | 7.00 |
| H100 × 50 × 4-40 | 260.59 | 0.16 | 0.96 | 1.54 | 9.63 |
| H100 × 50 × 4-70 | 280.51 | 0.16 | 0.83 | 1.17 | 7.31 |
| H100 × 50 × 4-110 | 274.45 | 0.15 | 0.55 | 0.90 | 6.00 |
| H50 × 100 × 4-0 | 78.62 | 0.24 | 0.46 | 0.66 | 2.75 |
| H50 × 100 × 4-40 | 84.50 | 0.29 | 1.16 | 1.26 | 4.34 |
| H50 × 100 × 4-40R | 85.52 | 0.29 | 1.05 | 1.32 | 4.55 |
| H50 × 100 × 4-70 | 89.13 | 0.29 | 1.19 | 1.46 | 5.03 |
| H50 × 100 × 4-110 | 88.89 | 0.30 | 1.18 | 1.40 | 4.67 |
| H140 × 140 × 5–0 | 1408.50 | 0.07 | 0.08 | 0.13 | 1.86 |
| H140 × 140 × 5–40 | 1567.77 | 0.09 | 0.26 | 0.44 | 4.89 |
| H140 × 140 × 5–70 | 1555.97 | 0.09 | 0.27 | 0.46 | 5.11 |
| H140 × 140 × 5–110 | 1547.98 | 0.09 | 0.23 | 0.43 | 4.78 |
| V80 × 80 × 4-0 | 211.67 | 0.21 | 0.41 | 0.55 | 2.62 |
| V80 × 80 × 4-40 | 231.66 | 0.23 | 0.80 | 0.92 | 4.00 |
| V80 × 80 × 4-70 | 233.46 | 0.22 | 0.71 | 0.84 | 3.82 |
| V80 × 80 × 4-110 | 230.01 | 0.23 | 0.63 | 0.76 | 3.30 |
| V100 × 100 × 4-0 | 343.07 | 0.16 | 0.22 | 0.28 | 1.75 |
| V100 × 100 × 4-40 | 416.67 | 0.17 | 0.44 | 0.54 | 3.18 |
| V100 × 100 × 4-70 | 429.26 | 0.17 | 0.45 | 0.57 | 3.35 |
| V100 × 100 × 4-70R | 422.56 | 0.17 | 0.48 | 0.60 | 3.53 |
| V100 × 100 × 4-110 | 427.66 | 0.17 | 0.44 | 0.53 | 3.12 |
| V120 × 120 × 4-0 | 838.03 | 0.09 | 0.11 | 0.17 | 1.89 |
| V120 × 120 × 4-40 | 858.77 | 0.13 | 0.22 | 0.33 | 2.54 |
| V120 × 120 × 4-70 | 857.32 | 0.14 | 0.28 | 0.34 | 2.43 |
| V120 × 120 × 4-110 | 855.36 | 0.13 | 0.23 | 0.29 | 2.23 |

Note: $\kappa_u$ is taken as the maximum recorded curvatures if the beams exhibited excessive deformations while sustained at the ultimate load until fracture of the steel tubes or the tests terminated.

the composite section. In the calculation of moment resistance, the limiting stresses are taken as yield stress $f_y$ in structural steel in tension or compression; and $0.85f_{cd}$ in concrete in compression; the stress in concrete in tension is ignored. The design concrete strength $f_{cd}$ is specified as $f_{cd} = f_{ck}/\gamma_C$, where $\gamma_C$ is a partial factor. Since $\gamma_C$ was omitted from this study for a direct comparison, the limiting stress in concrete in compression was taken as $0.85f'_c$. In this case, the Eurocode 4 [30] design rule and the comparison results against the test specimens are the same as those of AISC [31] in the previous section.

## 6. Conclusions

The paper presents an experimental study on flexural behaviour of concrete-filled steel tubular (CFST) members consist of high strength steel (HSS) tubes filled with normal and high strength concrete. Steel tubes of rectangular and square hollow sections were investigated. The measured 0.2% proof stresses of steel tubes were ranged from 682–1022 MPa and ultimate tensile strengths were ranged from 819–1179 MPa, while the average measured concrete cylinder strengths were 46.2, 71.2 and 117.0 MPa. It should be noted that some of these high strength materials are not covered in any design codes. Flexural strengths of concrete-filled specimens were compared with those hollow specimens without concrete infill. Ultimate moments of concrete-filled beams were found to be 9%–45% larger than those of hollow beams. The moment capacity slightly increases as the concrete strength increases. Generally, the influence of concrete strengths is more obvious on specimens with larger depth-to-thickness ($D/t$) ratio. A significant improvement on ductility of CFST beams has been observed compared with those hollow specimens. The test strengths were also compared with the design strengths calculated from the AISC Specification and European Code 4 for composite concrete–steel beams. The test specimens are all classified as compact sections in AISC Specification, and thus calculations for the flexural strengths by both design rules are identical for compact sections, which assume plastic stress distribution and maximum concrete strength of $0.85f'_c$. It is shown that such design approach provides conservative prediction for flexural strengths by 18% compared with the test results of concrete-filled high strength steel RHS and SHS beams.

## CRediT authorship contribution statement

**Yun-Qiao Deng:** Writing – original draft, Methodology, Data curation, Conceptualization. **Yuner Huang:** Writing – review & editing, Methodology, Investigation. **Ben Young:** Writing – review & editing, Supervision, Project administration, Funding acquisition, Conceptualization.

## Declaration of competing interest

The authors declare that they have no known competing financial interests or personal relationships that could have appeared to influence the work reported in this paper.

## Data availability

Data will be made available on request.

## References


[1] P. Levi, Tracking Industry 2020, International Energy Agency, 2020.

[2] L. Han, W. Li, R. Bjorhovde, Developments and advanced applications of concrete-filled steel tubular (CFST) structures: members, J. Construct. Steel Res. 100 (2014) 211–228, http://dx.doi.org/10.1016/j.jcsr.2014.04.016.

[3] K. Sakino, H. Nakahara, S. Morino, I. Nishiyama, Behavior of centrally loaded concrete-filled steel-tube short columns, J. Struct. Eng. 130 (2) (2004) 180–188, http://dx.doi.org/10.1061/(ASCE)0733-9445(2004)130:2(180).

[4] M. O'Shea, R. Bridge, Design of circular thin-walled concrete filled steel tubes, J. Struct. Eng. 126 (11) (2000) 1295–1303, http://dx.doi.org/10.1061/(ASCE)0733-9445(2000)126:11(1295).

[5] L. Han, Tests on stub columns of concrete-filled RHS sections, J. Construct. Steel Res. 58 (3) (2002) 353–372, http://dx.doi.org/10.1016/S0143-974X(01)00059-1.

[6] V. Kloppel, W. Goder, An investigation of the load carrying capacity of concrete-filled steel tubes and development of design formula, Der Stahlbau 26 (2) (1957) 44–50.

[7] C. Roeder, D. Lehman, E. Bishop, Strength and stiffness of circular concrete-filled tubes, J. Struct. Eng. 136 (12) (2010) 1545–1553, http://dx.doi.org/10.1061/(ASCE)ST.1943-541X.0000263.

[8] B. Young, E. Ellobody, Experimental investigation of concrete-filled cold-formed high strength stainless steel tube columns, J. Construct. Steel Res. 62 (5) (2006) 484–492, http://dx.doi.org/10.1016/j.jcsr.2005.08.004.

[9] S. Schneider, Axially loaded concrete-filled steel tubes, J. Struct. Eng. 124 (10) (1998) 1125–1138, http://dx.doi.org/10.1061/(ASCE)0733-9445(1998)124:10(1125).

[10] A. Varma, J. Ricles, R. Sause, L.-W. Lu, Experimental behavior of high strength square concrete-filled steel tube beam–columns, J. Struct. Eng. 128 (3) (2002) 309–318, http://dx.doi.org/10.1061/(ASCE)0733-9445(2002)128:3(309).

[11] T. Fujimoto, A. Mukai, I. Nishiyama, K. Sakino, Behavior of eccentrically loaded concrete-filled steel tubular columns, J. Struct. Eng. 130 (2) (2004) 203–212, http://dx.doi.org/10.1061/(ASCE)0733-9445(2004)130:2(203).

[12] M. Abramski, Load-carrying capacity of axially loaded concrete-filled steel tubular columns made of thin tubes, Arch. Civ. Mec. Eng. 18 (3) (2018) 902–913, http://dx.doi.org/10.1016/j.acme.2018.01.002.

[13] J.G. Teng, J.J. Wang, G. Lin, J. Zhang, P. Feng, Compressive behavior of concrete-filled steel tubular columns with internal high-strength steel spiral confinement, Adv. Struct. Eng. 24 (8) (2021) 1–22, http://dx.doi.org/10.1177/1369433220981656.

[14] H.-S. Hu, H.-Z. Wang, Z.-X. Guo, B.M. Shahrooz, Axial compressive behavior of square spiral-confined high-strength concrete-filled steel-tube columns, J. Struct. Eng. 146 (7) (2020a) 04020136, http://dx.doi.org/10.1061/(ASCE)ST.1943-541X.0002702.

[15] H.-S. Hu, L. Xu, Z.-X. Guo, B.M. Shahrooz, Behavior of eccentrically loaded square spiral-confined high-strength concrete-filled steel tube columns, Eng. Struct. 216 (2020b) 110743, http://dx.doi.org/10.1016/j.engstruct.2020.110743.

[16] J. Moon, C.W. Roeder, D.E. Lehman, H.-E. Lee, Analytical modeling of bending of circular concrete-filled steel tubes, Eng. Struct. 42 (2012) 349–361, http://dx.doi.org/10.1016/j.engstruct.2012.04.028.

[17] M. Elchalakani, X. Zhao, R. Grzebieta, Concrete-filled circular steel tubes subjected to pure bending, J. Construct. Steel Res. 57 (11) (2001) 1141–1168, http://dx.doi.org/10.1016/S0143-974X(01)00035-9.

[18] W. Gho, D. Liu, Flexural behaviour of high-strength rectangular concrete-filled steel hollow sections, J. Construct. Steel Res. 60 (11) (2004) 1681–1696, http://dx.doi.org/10.1016/j.jcsr.2004.03.007.

[19] L. Han, Flexural behaviour of concrete-filled steel tubes, J. Construct. Steel Res. 60 (2) (2004) 313–337, http://dx.doi.org/10.1016/j.jcsr.2003.08.009.

[20] H. Jiao, X. Zhao, Section slenderness limits of very high strength circular steel tubes in bending, Thin-Walled Struct. 42 (9) (2004) 1257–1271, http://dx.doi.org/10.1016/j.tws.2004.03.020.

[21] A. Kwan, Use of condensed silica fume for making high-strength, self-consolidating concrete, Can. J. Civil Eng. 27 (4) (2000) 620–627, http://dx.doi.org/10.1139/L99-091.

[22] F. Aslani, B. Uy, Z. Tao, F. Mashiri, Behaviour and design of composite columns incorporating compact high-strength steel plates, J. Construct. Steel Res. 107 (2015) 94–110, http://dx.doi.org/10.1016/j.jcsr.2015.01.005.

[23] Y. Du, Z. Chen, J. Liew, M.-X. Xiong, Rectangular concrete-filled steel tubular beam–columns using high-strength steel: Experiments and design, J. Construct. Steel Res. 131 (2017) 1–18, http://dx.doi.org/10.1016/j.jcsr.2016.12.016.

[24] D. Liu, Tests on high-strength rectangular concrete-filled steel hollow section stub columns, J. Construct. Steel Res. 61 (7) (2005) 902–911, http://dx.doi.org/10.1016/j.jcsr.2005.01.001.

[25] D. Liu, Behaviour of eccentrically loaded high-strength rectangular concrete-filled steel tubular columns, J. Construct. Steel Res. 62 (8) (2006) 839–846, http://dx.doi.org/10.1016/j.jcsr.2005.11.020.

[26] D. Liu, W.-M. Gho, J. Yuan, Ultimate capacity of high-strength rectangular concrete-filled steel hollow section stub columns, J. Construct. Steel Res. 59 (12) (2003) 1499–1515, http://dx.doi.org/10.1016/S0143-974X(03)00106-8.

[27] D. Liu, W.-M. Gho, Axial load behaviour of high-strength rectangular concrete-filled steel tubular stub columns, Thin-Walled Struct. 43 (8) (2005) 1131–1142, http://dx.doi.org/10.1016/j.tws.2005.03.007.

[28] H.-T. Thai, B. Uy, M. Khan, Z. Tao, F. Mashiri, Numerical modelling of concrete-filled steel box columns incorporating high strength materials, J. Construct. Steel Res. 102 (2014) 256–265, http://dx.doi.org/10.1016/j.jcsr.2014.07.014.

[29] A. Varma, J. Ricles, R. Sause, L.-W. Lu, Seismic behavior and design of high-strength square concrete-filled steel tube beam columns, J. Struct. Eng. 130 (2) (2004) 169–179, http://dx.doi.org/10.1061/(ASCE)0733-9445(2004)130:2(169).

[30] CEN (European Committee for Standardization, Design of Composite Steel and Concrete Structures, Part 1.1. Eurocode 4, CEN, Brussels, Belgium, 2004.

[31] AISC (American Institute of Steel Construction), Specification for Structural Steel Buildings, AISC 360-16, AISC, Chicago, Illinois, 2016.

[32] DBJ/T (The Housing and Urban-Rural Development Department of Fujian Province), Technical Specificatios for Concrete-Filled Steel Tubular Structures, DBJ/T 13-51, DBJ/T, Fuzhou, China, 2010, [in Chinese].

[33] Q.Q. Liang, High strength circular concrete-filled steel tubular slender beam–columns, Part I: Numerical analysis, J. Construct. Steel Res. 67 (2) (2011) 164–171, http://dx.doi.org/10.1016/j.jcsr.2010.08.006.

[34] Q.Q. Liang, High strength circular concrete-filled steel tubular slender beam–columns, Part II: Fundamental behavior, J. Constr. Steel Res. 67 (2) (2011) 172–180, http://dx.doi.org/10.1016/j.jcsr.2010.08.007.

[35] J.R. Liew, M. Xiong, D. Xiong, Design of high strength concrete filled tubular columns for tall buildings, Int. J. High-Rise Build. 3 (3) (2014) 215–221, http://dx.doi.org/10.21022/IJHRB.2014.3.3.215.

[36] G. Li, Z. Qiu, Z. Yang, B. Chen, Y. Feng, Seismic performance of high strength concrete filled high strength square steel tubes under cyclic pure bending, Adv. Steel Constr. 16 (2) (2020) 112–123, http://dx.doi.org/10.18057/IJASC.2020.16.2.3.

[37] B. Uy, Strength of short concrete filled high strength steel box columns, J. Construct. Steel Res. 57 (2) (2001) 113–134, http://dx.doi.org/10.1016/S0143-974X(00)00014-6.

[38] DB/T (The Urban-Rural Development Department of Tianjin), Technical Specification for Design of Steel Structure Dwelling Houses in Tianjin, DB/T 29-57, DB/T, Tianjin, China, 2016, [in Chinese].

[39] K. Chung, J. Kim, J. Yoo, Experimental and analytical investigation of high-strength concrete-filled steel tube square columns subjected to flexual loading, Steel Compos. Struct. 14 (2) (2013) 133–153, http://dx.doi.org/10.12989/scs.2013.14.2.133.

[40] G. Li, D. Liu, Z. Yang, C. Zhang, Flexural behavior of high strength concrete filled high strength square steel tube, J. Construct. Steel Res. 28 (2017) 732–744, http://dx.doi.org/10.1016/j.jcsr.2016.10.007.

[41] Y. Zhong, Y. Sun, K.H. Tan, O. Zhao, Testing, modelling and design of high strength concrete-filled high strength steel tube (HCFHST) stub columns under combined compression and bending, Eng. Struct. 241 (2021) 112334, http://dx.doi.org/10.1016/j.engstruct.2021.112334.

[42] Y. Zhong, K. Jiang, O. Zhao, Post-fire behaviour and capacity of high strength concrete-filled high strength steel tube (HCFHST) stub columns under combined compression and bending, Eng. Struct. 253 (2022) 113837, http://dx.doi.org/10.1016/j.engstruct.2021.113837.

[43] Y. Zhong, O. Zhao, Concrete-filled high strength steel tube stub columns after exposure to fire: Testing, numerical modelling and design, Thin-Walled Struct. 177 (2022) 109428, http://dx.doi.org/10.1016/j.tws.2022.109428.

[44] BSI (British Standard Institute), Design of Steel Structures, Part 1.1. Eurocode 3, BSI, London, UK, 2005.

[45] BSI (British Standard Institute), Metallic Products – Types of Inspection Documents, BS EN 10204, BSI, London, UK, 2004.

[46] BSI (British Standard Institute), Specification for Portland Cement, BS 12, BSI, London, UK, 1996.

[47] AS (Standards Australia), Metallic Materials - Tensile Testing at Ambient Temperature, AS 1391, AS, Sydney, Australia, 2007.

[48] ASTM (American Society for Testing and Material), Standards Test Methods for Tension Testing of Metallic Materials, E8/E8M-13a, ASTM, West Conshohocken, 2013.

[49] Y. Huang, B. Young, The art of coupon tests, J. Construct. Steel Res. 96 (2014) 159–175, http://dx.doi.org/10.1016/j.jcsr.2014.01.010.

[50] CEN (European Committee for Standardization), Metallic Materials - Tensile Testing Part 1: Method of Test at Ambient Temperature, ISO 6892-1, CEN, Brussels, Belgium, 2009.

[51] E. Krempl, F. Khan, Rate (time)-dependent deformation behavior: an overview of some properties of metals and solid polymers, Int. J. Plast. 19 (7) (2003) 1069–1095, http://dx.doi.org/10.1016/S0749-6419(03)00002-0.

[52] J.-L. Ma, T.-M. Chan, B. Young, Experimental investigation on stub-column behavior of cold-formed high-strength steel tubular sections, J. Struct. Eng. ASCE 142 (5) (2016) 04015174-1, http://dx.doi.org/10.1061/(ASCE)ST.1943-541X.0001456.

[53] J.Y.K. Lam, J.C.M. Ho, A.K.H. Kwan, Flexural ductility of high-strength concrete columns with minimal confinement, Mater. Struct. 42 (2009) 909–921, http://dx.doi.org/10.1617/s11527-008-9431-5.